



A fine-ordered nanostructured bismuth tin oxide thin film constructed via sol–gel nanopatterning for liquid crystal system

Dong Wook Lee¹ · Dong Hyun Kim¹ · Jin Young Oh¹ · Dae-Shik Seo¹

Received: 30 November 2021 / Accepted: 29 December 2021 / Published online: 12 January 2022
© The Author(s), under exclusive licence to Springer-Verlag GmbH, DE part of Springer Nature 2022

Abstract

Nanoimprint lithography is a very convenient and cost-effective method, and when combined with a sol–gel process, can be used to simply accomplish the nanopatterning of a bismuth tin oxide (BTO) film. We achieved the transfer of a nanostructure to a solution-driven BTO film by using nanoimprint lithography for utilization as a liquid crystal (LC) alignment layer. A curing temperature of 250 °C was ideal for the transfer of the nanopattern from polydimethylsiloxane to a BTO film, as confirmed by using atomic force microscopy, scanning electron microscopy, and x-ray photoelectron spectroscopy. The nanopattern led to the uniform alignment of LC molecules, as confirmed via polarized optical microscopy and pretilt angle analysis. In addition, the nanopattern-imprinted BTO film showed great potential for LC applications due to its high thermal stability and optical transmittance, along with super-fast switching and low voltage operating electro-optical characteristics. Sol–gel nanopatterning of metal oxides is a convenient process to create LC-alignment films for application in diverse electro-optical devices.

Keywords Bismuth tin oxide · Nanoimprint lithography · Sol–gel process · Nanostructure · Liquid crystal alignment · Electro-optical characteristic

1 Introduction

Uniform orientation of the liquid crystal (LC) is one of the most important technological processes for realizing high-quality LC applications, including displays [1–4]. Since LCs act as a light shutter, their uniform orientation can transmit or block (on or off) the light and show the digital image information. If the LCs are not uniformly aligned, the light through them is scattered, and so they cannot properly provide digital information nor completely block the light and provide high-quality images. Therefore, it is crucial to control light transmission through the orientation of the LCs [5]. Many techniques for LC alignment have been reported, such as rubbing [3, 6], ultraviolet exposure [7], evaporation [8], photo-alignment [9], sputtering [10], ion-beam exposure [11], and nanoimprinting lithography (NIL) [12]. Rubbing is the standard industrial technique for LC alignment due to its convenience,

cost-effectiveness, and uniform quality [13]. However, it has some drawbacks such as local defects, generation debris, and electrostatic discharge [14]. Other methods are expensive and/or complex. Among these, NIL provides the freedom to control the LC-alignment properties such as anchoring energy and pretilt angle [15–19]. Moreover, once the pattern is created, it can be used consistently and cost-effectively.

In this study, we achieved uniform LC alignment by using NIL combined with a sol–gel method; both methods are well-matched from the perspectives of cost-effectiveness and large-area processing [20, 21]. We used bismuth tin oxide (BTO), which has been used as gas sensors, anodes, and thin-film transistors [22–24], as an alignment layer. Although bismuth has high electron mobility due to the high degree of overlap in its wave function, it also hinders the formation of the crystalline structures, thereby making it exhibit unique electrical and optical properties [25, 26]. The aligned nanopattern used in NIL was fabricated on silicon wafer by using laser interference lithography (LIL), which is very simple and fast [27, 28]. The well-ordered nanopattern was then transferred to polydimethylsiloxane (PDMS) sheet for application as a master cast. The negative replica nanopattern on master cast was subsequently imprinted with BTO in the sol state followed by curing at 70,

✉ Dae-Shik Seo
dsseo@yonsei.ac.kr

¹ IT Nano Electronic Device Laboratory, Department of Electrical and Electronic Engineering, Yonsei University, Seodaemun-gu, Seoul 120-749, South Korea

160, or 250 °C to produce thin films. The uniformity of LC alignment with the BTO nanopattern was investigated by using polarized optical microscopy (POM), while the pretilt angle of the LC molecules was measured via a crystal rotation method [29]. The surface morphology of the nanopattern-imprinted BTO film was measured by using atomic force microscopy (AFM) and field emission scanning electron microscope (SEM), while its chemical structure was observed via X-ray photoelectron spectroscopy (XPS). The thermal stability of LCs on a nanopattern-imprinted BTO film was investigated via an annealing process with POM analysis. Contact angle measurements and X-ray diffraction (XRD) analysis were progressed to examine the crystallinity and chemical affinity of the nanopattern-imprinted BTO film. Optical transmittance was measured via UV–visible–near infrared (UV–Vis–NIR) spectroscopy. The applicability of nanopattern-imprinted BTO was considered via assessing its electro-optical performance in a twisted nematic (TN)-LC system.

2 Experimental details

2.1 Fabrication of the LC-alignment nanopattern and preparation of a polydimethylsiloxane (PDMS) mold

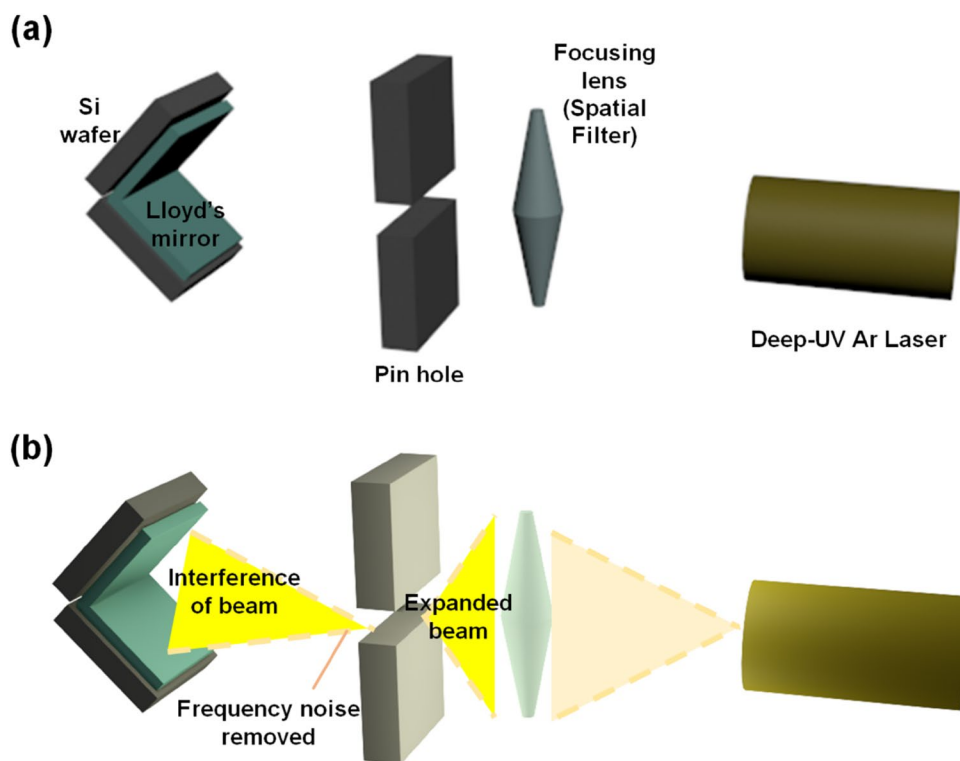
A 257-nm Ar laser and a single-beam Lloyd's mirror interferometer were used for fabricating the initial periodic

nanostructures on a silicon (Si) wafer. The deep UV LIL process is illustrated in Fig. 1. The laser wavelength was doubled by using beta-barium borate crystals, and for dose uniformity, the beam was expanded by a factor of 27 in the spatial filter. A focusing lens and pinhole were used as a filter and the spatial frequency noise was removed at the filter. After that, coherent light sequentially applied to the pinhole was emitted, reached both sides of the Si wafer and Lloyd's mirror, and was reflected on the Si wafer. This induced interference of the light applied to both sides, which fabricated the nanopattern on the Si wafer with a pitch of 750 nm and a height of 30 nm. A flexible mold was prepared by mixing a PDMS base and a curing agent (the Sylgard-184 elastomer kit, Dow Corning) that was then poured onto the nanopatterned Si wafer; the flexibility of the PDMS ensured conformal contact between the nanopattern and the BTO film. During the imprinting process, the nanopatterned PDMS was placed onto the as-deposited sol film, after which the heat was applied. The underlying liquid sol rose and filled the nanopattern structure via capillary pressure and was then solidified by the heat.

2.2 Preparation of the BTO solution via a sol–gel method and imprinting of the nanopattern on the BTO film

A 0.1 M BTO solution was prepared by dissolving in(II) chloride (SnCl_2 ; $\geq 99.99\%$, trace metals basis), and bismuth(III)

Fig. 1 Schematics of the fabrication of the 1-dimensional nanostructure on a silicon wafer by laser interference lithography. **a** Before and **b** after laser treatment



nitrate pentahydrate ($\text{Bi}(\text{NO}_3)_3 \cdot 5\text{H}_2\text{O}$; $\geq 98.0\%$, ACS Reagent Chemicals) with a Bi:Sn molar ratio of 1:1 in 2-methoxy ethanol (2ME). The solution was then stirred for 2 h at 80 °C using a magnetic stirrer, and then aged for 1 day. The prepared BTO solution was spin-coated onto the glass substrate at a spin rate of 3000 rpm for 30 s. The nanopatterned PDMS mold was placed onto the spin-coated BTO film at curing temperatures of 70, 160, or 250 °C, and the nanostructure was transferred onto the BTO film. The entire imprinting process (including fabrication of the PDMS mold) is illustrated in Fig. 2a.

2.3 Characteristics of the nanopattern-imprinted BTO film

The surface morphologies of the nanopattern-imprinted BTO films were investigated by using AFM (XE-BIO, Park Systems,) and field emission SEM (S-4300SE, Hitachi), while their chemical compositions were measured via XPS (K-alpha, Thermo VG). Contact angle measurements were conducted via the sessile drop technique with deionized (DI) water and diiodomethane by using a phoenix 300 surface angle analyzer, followed by analysis with IMAGE PRO 300 software. An investigation of the film structures

was performed by using XRD (DMAX-III A, Rigaku). Optical transmittance was measured in accumulation mode 3 times in the range of 250–850 nm at room temperature by using a UV–vis–NIR spectrophotometer (V-650, JASCO Corporation).

2.4 LC cell fabrication for LC alignment status and electro-optical performance evaluation

We assembled anti-parallel LC cells with a cell gap of 60 μm using a nanopattern-imprinted BTO film as the LC-alignment layer. Positive LCs (IAN-5000XX T14, $\Delta n = 0.111$, $n_e = 1.595$, $n_o = 1.484$; JNC) were injected between each pair of substrates along the direction parallel to the pattern. The expected LC-alignment status of the 1-dimensional nanostructure is illustrated in Fig. 2b. POM (BXP 51, Olympus) was used to confirm the uniformity of the LC alignment in the cell and the thermal stability of the nanopattern-imprinted BTO layer. A crystal rotation method (TBA 107, Autronic) was used to measure the pretilt angle of the LCs on the nanopattern-imprinted BTO layer. A TN-LC cell was assembled with a 5 μm cell gap to investigate the electro-optical characteristics of the nanopattern-imprinted BTO layer. A TN-LC cell with a conventional homogeneous

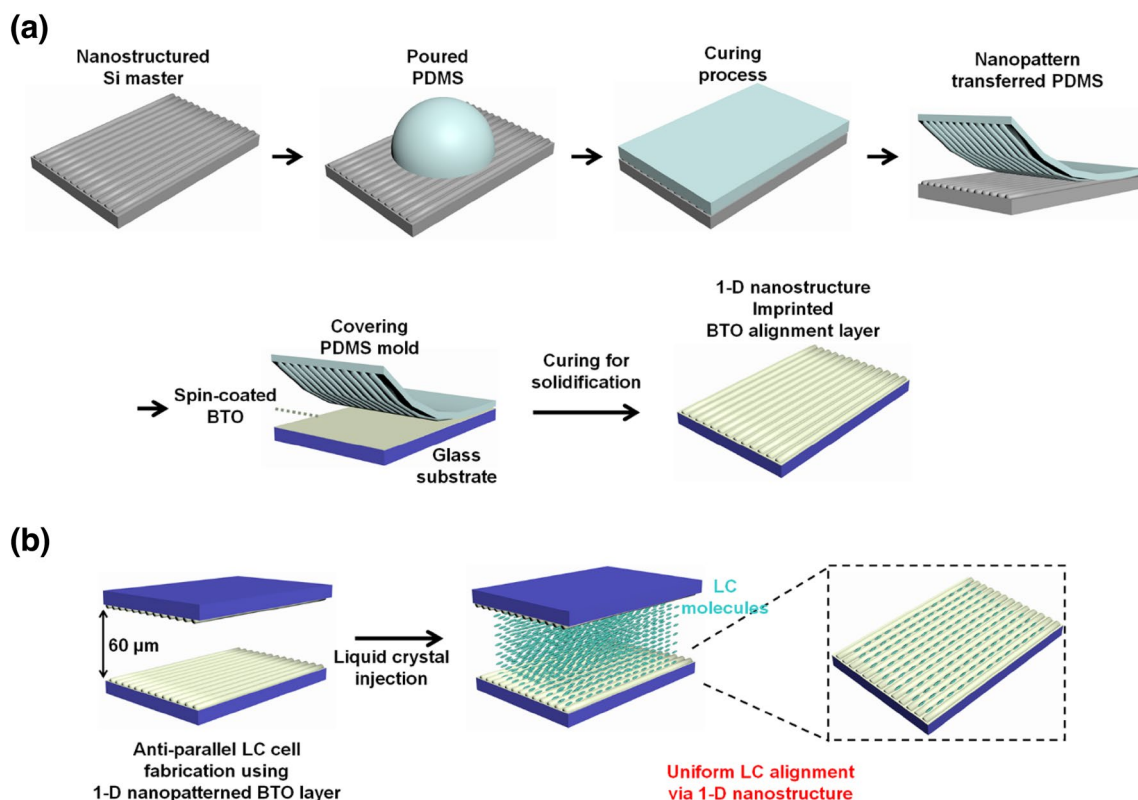


Fig. 2 **a** A schematic of the transfer of the 1-dimensional nanostructure from the nanopatterned silicon wafer to the bismuth tin oxide (BTO) alignment layer with a polydimethylsiloxane (PDMS) mold

via nanoimprinting lithography and curing. **b** A schematic of the alignment process of liquid crystals (LCs) on the BTO alignment layer in an anti-parallel LC cell to achieve uniform LC alignment

polyimide (PI) layer fabricated via rubbing (RN-1199A, Nissan Chemical Industries, Ltd., Tokyo, Japan) was also assembled for comparison of response times and voltage-transmittance (V-T) graphs measured using an LC display evaluation system (LCMS-200).

3 Results and discussion

We investigated the surface morphologies of BTO films according to curing temperatures by using AFM and SEM analyses to confirm the successful transfer of the nanopattern from the PDMS mold to the BTO film (Fig. 3). The PDMS master mold was also investigated for comparison. As can be seen in 3D and top-view topological AFM images in Fig. 3a, the nanopattern began to appear as the curing temperature was increased; we can see that the nanopattern was clearly generated in the 250 °C-cured BTO film. This result indicates that heat is an important factor for successful nanopattern transfer. For a more specific analysis, the SEM image of the surface and the line profile data of the film and PDMS mold are shown in Fig. 3b. The SEM image also shows the 1-dimensional nanopattern on the 250 °C-cured BTO film surface, which consisted of the gel state of BTO. The PDMS mold showed well-defined nanopattern line profiles with a pitch of 750 nm, a width of 230 nm (measured at 90% of the height), and a height of 12 nm originating from the Si master wafer. Although the line profiles on the 250 °C-cured BTO film were similar, the feature sizes were slightly decreased. When the nanopattern was transferred to the BTO film from the PDMS mold, the PDMS was placed onto the BTO layer in the sol state during the curing process. The BTO in the sol state rose to fill the PDMS nanopattern via capillary pressure. The upper side of the nanopatterned PDMS was filled by BTO solution from underneath, which was then solidified by the heat treatment. Therefore, as aforementioned, heat treatment is important for successful nanopattern construction, and a sufficiently high curing temperature is required to construct solid BTO-derived nanopatterns. The nanopattern constructed on the 250 °C-cured BTO film surface indicates that the sol state of BTO film was completely transformed into the gel state via dehydration at the curing temperature.

The BTO film was fabricated via a sol–gel method that depended on the curing temperature. A low curing temperature could leave residual solvent on the surface and thus could prevent our intended stoichiometric chemical modifications [28]. An XPS analysis was conducted on the 70 °C- and 250 °C-cured BTO films to investigate the chemical compositions of the nanopattern constructions, the results of which are shown in Fig. 4. The XPS survey scan was

conducted in the range of 100–600 eV, in which Bi 4f, C 1 s, Sn 3d, and O 1s peaks were observed for both films, thereby indicating the formation of the BTO film via the NIL process. There were distinct differences in the peak intensities of the main atoms between the samples, which indicates more active thermal oxidation on the surface of the film at the higher temperature. Thus, the BTO film was well-formed at a curing temperature of 250 °C rather than at 70 °C.

For the specific XPS analysis shown in Fig. 5, the Sn 3d spectra convoluted into Sn 3d 5/2 and Sn 3d 3/2 due to spin–orbit splitting shifted from 487.0 and 495.4 eV for the 70 °C-cured BTO film to 486.6 and 495.1 eV for the 250 °C-cured BTO film, respectively, due to oxidization of Sn atoms. The Bi 4f spectra comprised four peaks for the 70 °C-cured BTO film centered at 157.8, 159.7, 163.1, and 165.0 eV, which are assigned to Bi 4f 7/2 metal, Bi 4f 7/2 oxide, Bi 4f 5/2 metal, and Bi 4f 5/2 oxide, respectively [30, 31]. The presence of the Bi 4f 7/2 and Bi 4f 5/2 metal peaks indicates that curing at 70 °C was not sufficient to fully oxidize the metal bonds of the Bi atoms. On the other hand, Bi-metal peaks were not observed in the spectrum of the 250 °C-cured BTO film, with the two peaks centered at 159.4 eV and 164.7 eV indicating the presence of Bi 4f 7/2 oxide and Bi 4f 5/2 oxide, respectively. The negative shift in one of the sub-peaks in the O 1s spectra in the 70 °C- and 250 °C-cured BTO films from 530.5 to 530.2 eV was due to increasing metal–oxygen bonding via active thermal oxidation in the latter. In addition, the other sub-peak due to oxygen vacancies was dramatically increased in the 250 °C-cured BTO film compared to the 70 °C-cured BTO film. The C 1 s spectra comprised of three sub-peaks centered in the range of 284–285 eV, 285.5–286.5 eV, and 288–289 eV, respectively, which representing C–O, C–O–M (M = metal, i.e. Bi and Sn in this case), and C=O bonding, respectively. These spectra were attributed to the PDMS mold which covered BTO film when curing process. The sub-peaks were generally increased at higher curing temperature. Especially, the increased C–O–M peak indicates the more actively oxidized metal state on the 250 °C-cured film surface compared to 70 °C-cured film surface. The XPS results comprehensively show that the two metal atoms (Bi, and Sn) create more bonds with oxygen at the higher curing temperature, which contributes to the construction of the nanostructure on the BTO film surface.

To investigate the relationship between LC alignment and the 1-dimensional nanostructure, anti-parallel LC cells were fabricated with a nanoimprinted BTO layer cured at 70, 160, or 250 °C. The LC-alignment status was evaluated via POM analysis and pretilt angle measurements. As shown in the schematic in Fig. 6a, the orientation of the LC molecules

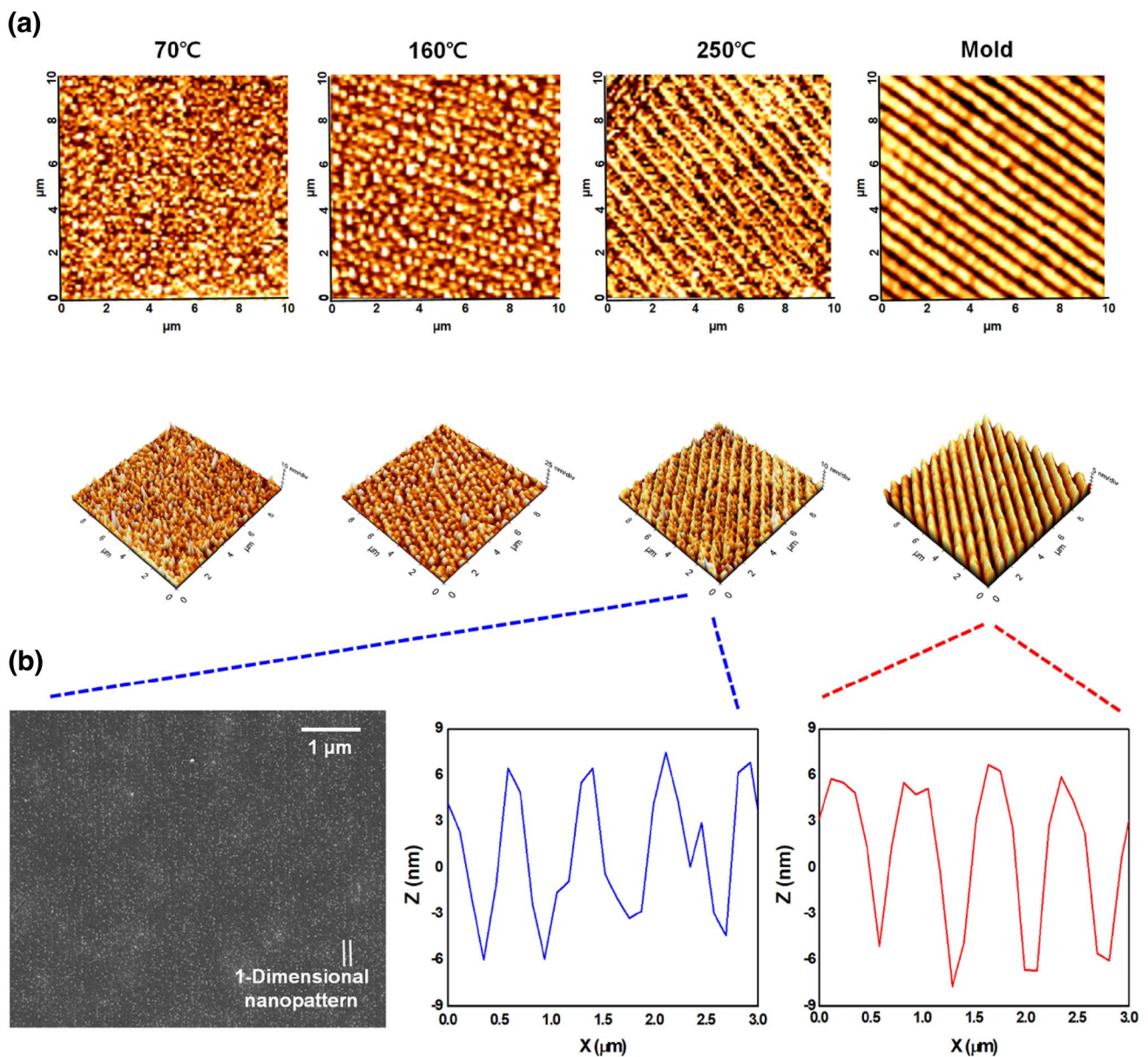


Fig. 3 **a** Top-view (upper) and 3-dimensional (lower) atomic force microscopy images of the surface morphologies of nanopattern-imprinted bismuth tin oxide (BTO) films according to curing temperatures. The polydimethylsiloxane (PDMS) master mold surface is

also shown for comparison. **b** An SEM image and line profile (red) of the nanopattern-imprinted BTO film cured at 250 °C. The line profile (blue) of the PDMS master mold is also shown for comparison

determines the light transmittance since the LC cells are positioned between the vertically crossed polarizer and analyzer. When the positive LCs are aligned uniformly, polarized backlight induced by the polarizer penetrates through the aligned LCs and is then blocked by the upper analyzer. Although a completely black POM image was obtained when using a 250 °C-cured BTO film (indicating that the

LCs were uniformly aligned), randomly distributed positive LCs when using a BTO film cured at 70 °C or 160 °C caused the polarized backlight to scatter, and so light could pass through the analyzer, resulting in the POM images not being completely black (Fig. 6b).

The oscillated transmittance curves of the LC cells measured via a crystal rotation method (Fig. 6c) demonstrate how

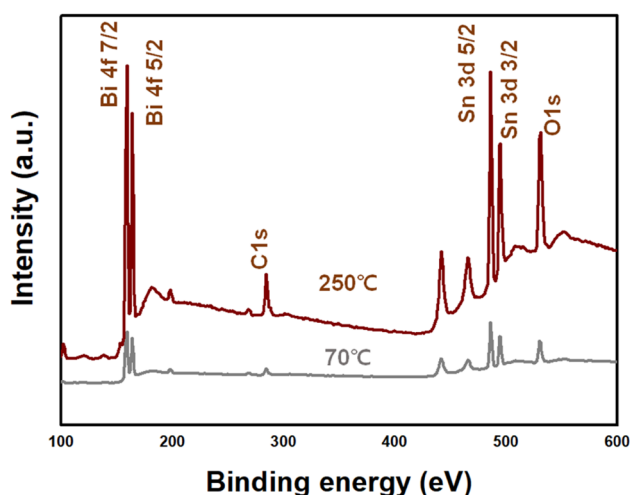


Fig. 4 X-ray photoelectron spectroscopy survey-scan spectra in the range of 100–600 eV to investigate the atomic compositions of the nanopattern-imprinted bismuth tin oxide films cured at 70 and 250 °C

well the LC molecules were uniformly aligned and were used to calculate the pretilt angle of the LCs. The transmittance was measured by projecting a light beam on the rotating LC cells. The blue curve represents the simulated data, and the red curve represents the data measured from LC cells. A good match between the simulated and real data curves indicates that the LC molecules are uniformly aligned with a stable pretilt angle, which can then be accurately calculated. However, a mismatch between the real data and simulated curves indicates that the LCs are randomly distributed and the pretilt angle of the LCs cannot be accurately estimated. Well-matched curves were obtained using the 250 °C-cured BTO layer, which was not the case for the BTO layers formed at curing temperatures of 70 and 160 °C, a result that supports the POM analysis findings. The pretilt angle of the LCs with the 250 °C-cured BTO layer was calculated as 0.031, which infers homogeneous LC alignment. These results correspond with our expectation of LC alignment by the unidirectional nanostructure. The LCs have elastic and liquid characteristics, which is attributed to the collective behavior induced by strong molecular interaction among the LC molecules. The elasticity is in the direction that minimizes the free energy of the LC bulk. Therefore, our 1-dimensional nanopattern can guide the direction of LCs by minimizing distortion.

Advanced LC applications for bright high-resolution displays require high thermal stability because of the numerous switching components. To test the thermal stability of an LC cell with a 250 °C-cured nanopattern-imprinted BTO, Fig. 7 shows POM images obtained after annealing it from

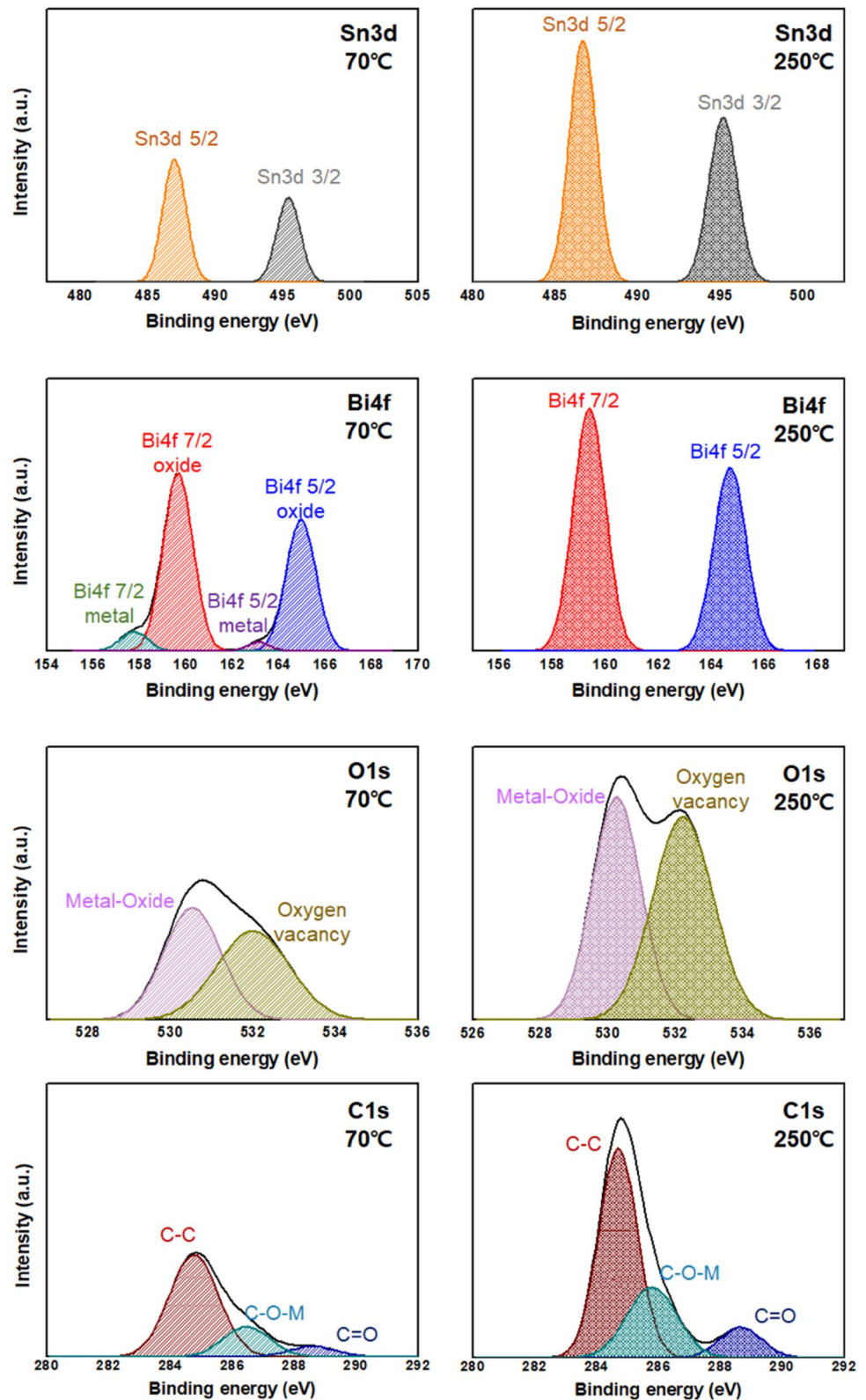
90 to 210 °C at 30 °C intervals for 10 min each. The LCs on the nanopattern-imprinted BTO film maintained uniform and homogeneous alignment up to 180 °C, which infers a remarkable thermal budget compared to that of conventional rubbed PI (150 °C). Therefore, nanopattern-imprinting of BTO film is a good candidate for advanced LC applications.

Contact angle measurements, and XRD and optical transparency analyses, were performed to investigate the characteristics of the nanopattern-imprinted BTO film. Contact angles measurements can give information about the chemical affinity of the measured surface and the contact angle is inversely proportional to the surface energy. The contact angles of nanopattern-imprinted BTO films at various curing temperatures are exhibited in Fig. 8, while the surface energies were calculated by using the DI water and diiodomethane contact angles by applying the Owen-Wendt method (Table 1) [32]. As the curing temperature was increased from 70 to 250 °C, the contact angle increased from 65.91° to 97.19° for DI water while the surface energy decreased from 43.9 to 29.36 mJ/m². These results are attributed to the effect of thermal oxidation of the PDMS that covered the BTO film during the curing process. At the same time, the 1-dimensional nanopattern was well-transferred on the suitably metal-oxidized BTO film at a curing temperature of 250 °C, which could induce uniform alignment of LC molecules on the surface with its hydrophobic properties.

XRD analysis was progressed in 2 θ scan mode from 20° to 80° to investigate the crystallinity of the nanopattern-imprinted BTO film cured at 250 °C, the results from which are presented in Fig. 9. The XRD spectrum does not show any major peaks, which means that the nanopattern-imprinted BTO film surface was amorphous, which is in agreement with the general finding that solution-processed oxide films produced with a curing temperature below 500 °C have an amorphous structure [33]. Although this result was as expected, we also demonstrated that LC alignment was not affected by the amorphous structure of the BTO film.

The optical transparency of a film is an important factor for LC systems. Transmittance graphs of the BTO films cured at 70, 160, and 250 °C in the wavelength range of 250–850 nm are shown in Fig. 10. The optical transparency values of both plain and indium tin oxide (ITO)-coated glass, and PDMS mold were also measured for comparison. In the visible wavelength band (in the range of 380–740 nm), the average optical transparency values of the 70-, 160-, and 250 °C-cured BTO films were calculated as 86.3%, 85.6%, and 87.6%. Those for the plain and ITO coated glass, and PDMS mold was calculated as 86.1%, 82.3%, and 86.3% respectively. These results indicate that

Fig. 5 High-resolution Sn 3d, Bi 4f, O 1s, and C 1s core-level X-ray photoelectron spectroscopy spectra of the bismuth tin oxide film surfaces cured at 70 and 250 °C



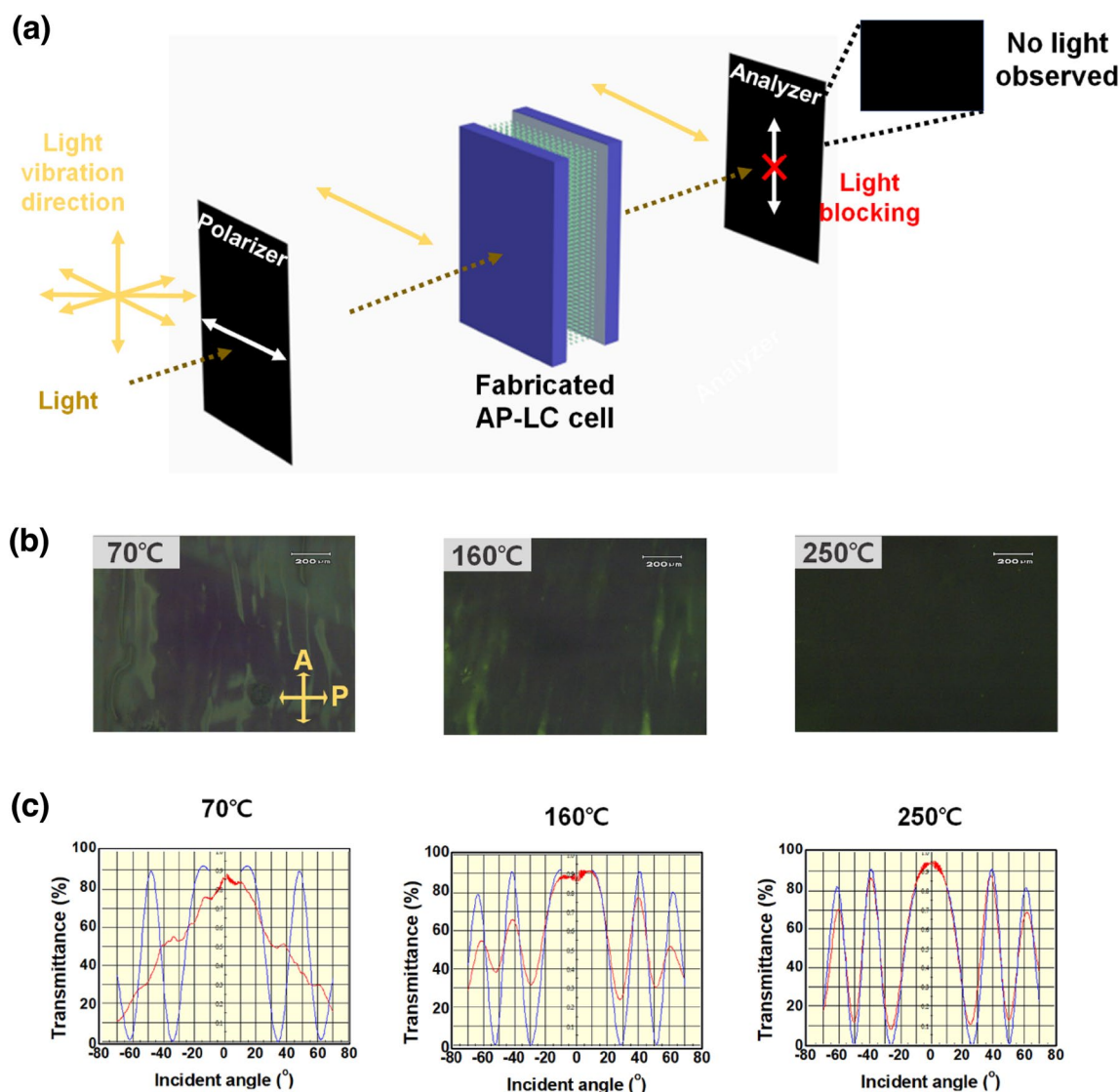


Fig. 6 **a** An illustration of the path and wave direction of light passing through the polarizer, an anti-parallel LC cell fabricated with a nanopattern-imprinted bismuth tin oxide (BTO) layer cured at 250 °C, and the analyzer. The wave direction of the light is divided into three main areas (before passing through the polarizer, between the polarizer and the anti-parallel LC cell, and between the anti-parallel LC cell and the analyzer). Unidirectional light is blocked in the analyzer, resulting in a dark image in the POM result. **b** Polarized optical microscopy images of the anti-parallel LC cells fabricated

with nanopattern-imprinted BTO alignment layers cured at 70, 160, or 250 °C. The directions of the polarizer (P) and analyzer (A) are denoted by the yellow arrows. **c** Transmittance curves of anti-parallel LC cells with a nanopattern-imprinted BTO layer cured at 70, 160, or 250 °C. The graphs are plotted versus latitudinal rotation from -70° to 70° using the crystal rotation method for the pretilt angle calculations. The blue curve represents the simulated data, and the red curve represents the data measured from the anti-parallel LC cells

the nanopattern-imprinted BTO film cured at 250 °C has competitive transparency compared to plain glass and PDMS mold. The horizontal curves in this region also infer the excellent optical stability of the BTO films. Thus, the optical transparency characteristics of the BTO film indicate that it is appropriate for use in LC applications.

A TN-LC cell was fabricated with a 250 °C-cured nanopattern-imprinted BTO film to confirm its practicability as an LC-alignment layer in LC applications. Evaluation of its electro-optical characteristics is given in Fig. 11. In a TN-LC system, the LCs are twisted at 90° and parallel to the upper and lower alignment layers with no applied voltage (the off

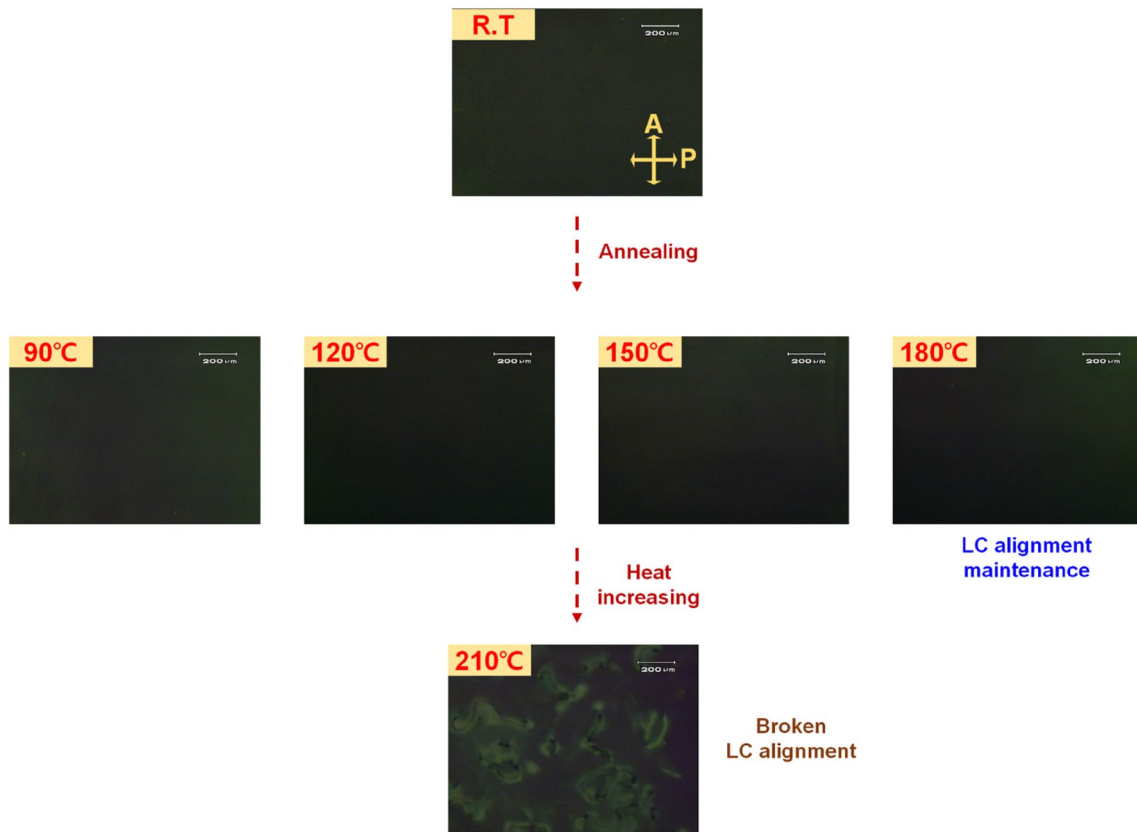


Fig. 7 Thermal stability testing of the LCs in anti-parallel LC cells based on nanopattern-imprinted bismuth tin oxide layer cured at 250 °C. The LC-alignment status was analyzed by using polarized optical microscopy (POM) and an annealing process from 90 to 210 °C with

30 °C intervals for 10 min each. A room temperature POM image is shown for comparison. The directions of the polarizer (P) and analyzer (A) are denoted by the yellow arrows in the first image

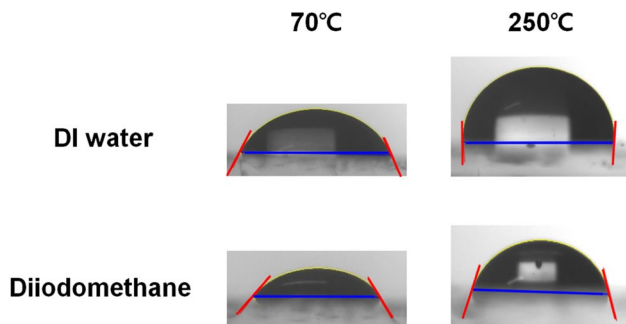


Fig. 8 Images used for contact angle measurements for drops of DI (deionized) water and diiodomethane on nanopattern-imprinted bismuth tin oxide films cured at 70 and 250 °C

Table 1 Contact angles measurements and calculated surface energies of the nanopattern-imprinted BTO films cured at 70 and 250 °C

Curing Temperature (°C)	Contact Angle (°)		Dispersive Energy (mJ/m ²)	Polar Energy (mJ/m ²)	Surface Snergy (mJ/m ²)
	DI* Water	Dii-dometh-ane			
70	65.91	54.64	31.65	12.24	43.90
250	97.19	60.29	28.41	0.95	29.36

*Deionized

state) whereas an applied voltage untwists them and turns them perpendicular to the alignment layers (the off state), as illustrated in Fig. 11a. The transition time from the off state to the on state of the LCs is defined as the rise time,

with the opposite being the fall time. The total response time (summation of the rise and fall times) is one of the most important considerations for an LC system as it measures how well the system can switch between the on and off states for controlling the passage of light. The rise and fall times of the TN cell based on the nanopattern-imprinted

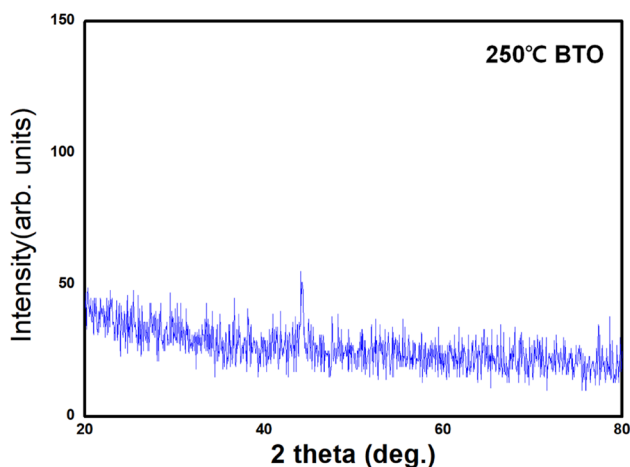


Fig. 9 An X-ray diffraction spectrum of a nanopattern-imprinted bismuth tin oxide film cured at 250 °C

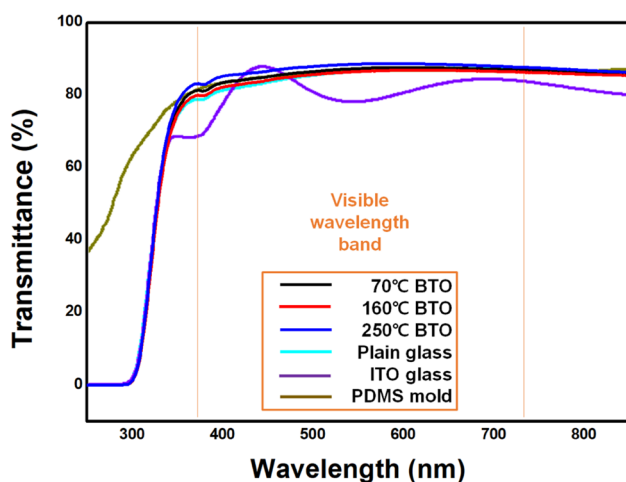


Fig. 10 Optical transparency graphs in the 250–850 nm wavelength range of nanopattern-imprinted bismuth tin oxide films cured at 70, 160, and 250 °C. Those for both plain and indium-tin-oxide-coated glass, and polydimethylsiloxane mold are included for comparison. The visible range is indicated by the orange solid lines

BTO film were calculated as 1.8 and 6.3 ms (Fig. 11b); the total response time of 8.1 ms is noteworthy short compared to conventional TN-LC systems based on PI layers [34] and is attributed to the dielectric properties of the bismuth and tin oxides [35–38]. Voltage-transmittance curves obtained to investigate the operating properties of nanopattern-imprinted BTO film-based TN-LC cells and compare them with a conventional cell with PI layers are shown in Fig. 11c. The threshold voltages (corresponding to 90% transmission) of TN-LC cells with nanopattern-imprinted BTO films and PI films were calculated as 1.2 and 1.8 V, respectively, thereby demonstrating the superior low voltage operation of the TN-LC system with the BTO film [39, 40]. This greatly reduced threshold voltage means decreased power consumption of LC systems during operation.

4 Conclusion

We successfully transferred a nanostructure from a PDMS mold to a solution-driven BTO film and cured it at 70, 160, or 250 °C. A clear imprint of the nanopattern was observed in the 250 °C-cured BTO film via AFM and SEM analyses. Chemical composition modification during the NIL process was confirmed by using XPS. The nanopattern on the BTO film was successfully used to align LC molecules uniformly, as evaluated via POM and pretilt angle measurements. The BTO alignment layer showed an excellent thermal budget for use in LC systems. The nanopattern-imprinted BTO film also had high optical transparency. TN-LC cells fabricated with BTO layers exhibited outstanding switching and low voltage operational electro-optical properties, which is essential for high-end LC systems. Thus, the use of our nanopattern-imprinted BTO film in advanced LC application is extremely encouraging, and the sol-gel nanopatterning using metal-oxide materials could be applied to diverse electro-optical devices.

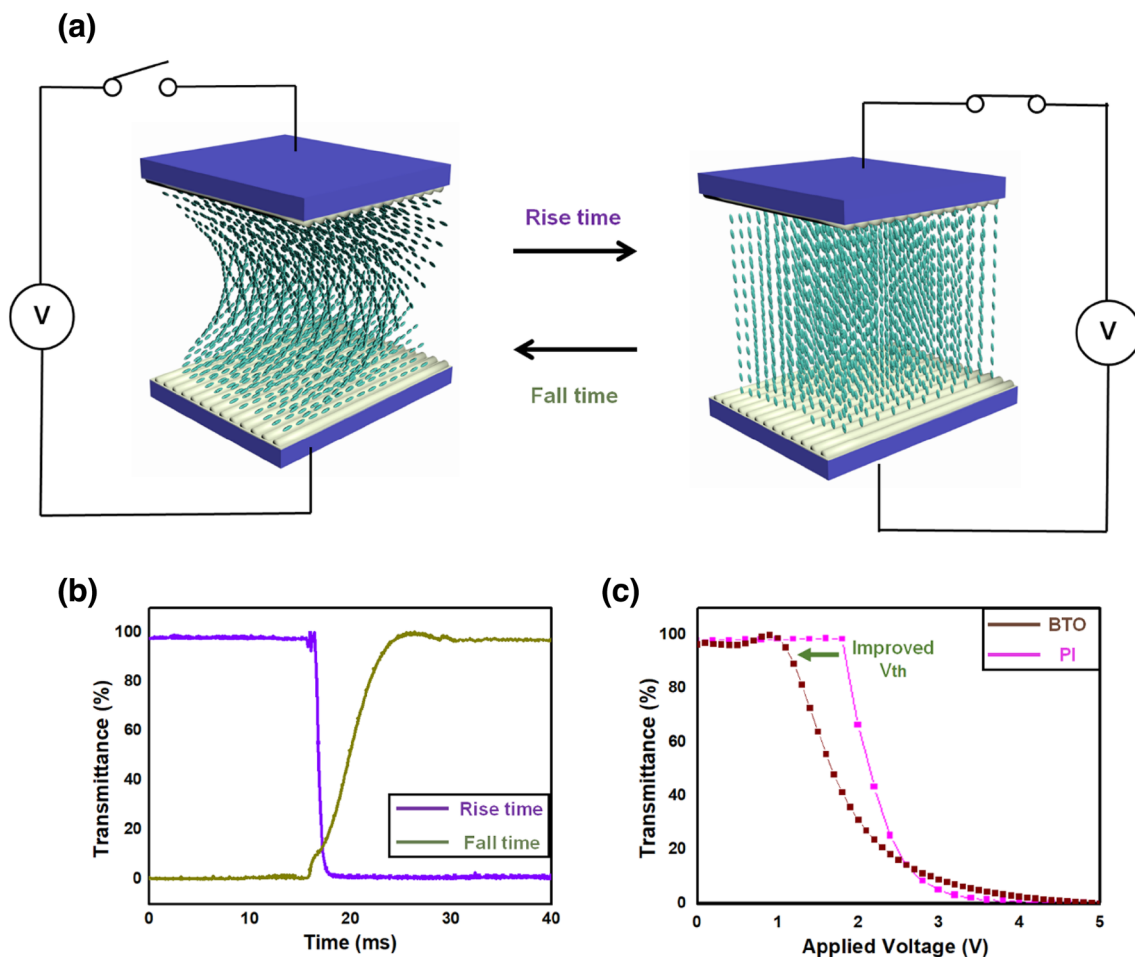


Fig. 11 **a** Illustrations of a twisted nematic (TN)-LC cell assembled with nanopattern-imprinted bismuth tin oxide (BTO) layers cured at 250 °C in the no voltage applied (off) state (left) and the voltage applied (on) state (right). The transition times between them are referred to as the rise time (off to on) and fall time (on to off). **b** The

response and fall times of the TN-LC with nanopattern-imprinted BTO layers cured at 250 °C. **c** Voltage-transmittance graphs of TN-LC cells made with NP BTO layers cured at 250 °C or conventionally used PI layers (for comparison)

Declarations

Conflict of interest The authors have no conflict of interest to declare that are relevant to the content of this article.

References

- M.F. Toney, T.P. Russell, J.A. Logan, H. Kikuchi, J.M. Sands, S.K. Kumar, Near-surface alignment of polymers in rubbed films. *Nature* **374**, 709 (1995)
- P. Chaudhari, J. Lacey, J. Doyle, E. Galligan, S.C.A. Lien, A. Callegary, G. Hougham, N.D. Lang, P.S. Andry, R. John, K.H. Yang, M. Lu, C. Cai, J. Speidell, S. Purushothaman, J. Ritsko, M. Samant, J. Stöhr, Y. Nakagawa, Y. Katoh, Y. Saitoh, K. Sakai, H. Satoh, S. Odahara, H. Nakano, J. Nakagaki, Y. Shiota, Atomic-beam alignment of inorganic materials for liquid-crystal displays. *Nature* **411**, 56 (2001)
- J. Stöhr, M.G. Samant, J. Lühning, A.C. Callegari, P. Chaudhari, J.P. Doyle, J.A. Lacey, S.A. Lien, S. Purushothaman, J.L. Speidell, Liquid crystal alignment on carbonaceous surfaces with orientational order. *Science* **292**, 2299 (2001)
- Y. J. Liu, W. W. Loh, E. S. P. Leong, T. S. Kustandi, X. W. Sun, J. H. Teng, Nanoimprinted ultrafine line and space nanogratings for liquid crystal alignment. *Nanotechnology* **23**, 465302 (2012)
- Z. Yan, J. Yao, Y. Hou, J. Zhou, J. Sun, X. Huang, Intermediate pre-tilt angle control by a composite alignment thin film structure for liquid crystal displays. *Appl. Phys. A* **127**, 82 (2021)
- Y.-D. Chen, K.-T. Cheng, C.-K. Liu, A.Y.-G. Fuh, Polarization rotators fabricated by thermally-switched liquid crystal alignments based on rubbed poly(N-vinyl carbazole) films. *Opt. Express* **19**, 7553 (2011)
- N. Kawatsuki, H. Ono, H. Takatsuka, T. Yamamoto, O. Sengen, Liquid crystal alignment on photoreactive side-chain liquid-crystalline polymer generated by linearly polarized UV light. *Macromolecules* **30**, 6680 (1997)
- K.A. Simon, E.A. Burton, F. Cheng, N. Varghese, E.R. Falcone, L. Wu, Y.-Y. Luk, Controlling thread assemblies of pharmaceutical

- compounds in liquid crystal phase by using functionalized nanotopography. *Chem. Mater.* **22**, 2434 (2010)
9. L. Zhang, Z. Peng, L. Yao, C. Fei, F. Lv, L. Xuan, Photoalignment of liquid crystals by cinnamate polyelectrolyte layer-by-layer ultrathin film. *Appl. Surf. Sci.* **253**, 3372 (2007)
 10. G.M. Wu, C.Y. Liu, A.K. Sahoo, RF sputtering deposited a-IGZO films for LCD alignment layer application. *Appl. Surf. Sci.* **354**, 48 (2015)
 11. Y.-G. Kang, H.-J. Kim, H.-G. Park, B.-Y. Kim, D.-S. Seo, Tin dioxide inorganic nanolevel films with different liquid crystal molecular orientations for application in liquid crystal displays (LCDs). *J. Mater. Chem.* **22**, 15969 (2012)
 12. I.H. Song, H.-C. Jeong, J.H. Lee, J. Won, D.H. Kim, D.W. Lee, J.Y. Oh, J.I. Jang, Y. Liu, D.-S. Seo, Selective liquid crystal driving mode achieved by controlling the pretilt angle via a nanopatterned organic/inorganic hybrid thin film. *Adv. Opt. Mater.* **9**, 2001639 (2021)
 13. K. Weiss, C. Wöll, E. Böhm, B. Fiebranz, G. Forstmann, B. Peng, V. Scheumann, D. Johannsmann, Molecular orientation at rubbed polyimide surfaces determined with X-ray absorption spectroscopy: relevance for liquid crystal alignment. *Macromolecules* **31**, 1930 (1998)
 14. J. Haaren, Wiping out dirty displays. *Nature* **411**, 29 (2001)
 15. R. Lin, J.A. Rogers, Molecular-scale soft imprint lithography for alignment layers in liquid crystal devices. *Nano Lett.* **7**, 1613 (2007)
 16. J.C. Armas-Pérez, X. Li, J.A. Martínez-González, C. Smith, J.P. Hernández-Ortiz, P.F. Nealey, J.J. de Pablo, Sharp morphological transitions from nanoscale mixed-anchoring patterns in confined nematic liquid crystals. *Langmuir* **33**, 12516 (2017)
 17. D.-R. Chiou, L.-J. Chen, C.-D. Lee, Pretilt angle of liquid crystals and liquid-crystal alignment on microgrooved polyimide surfaces fabricated by soft embossing method. *Langmuir* **22**, 9403 (2006)
 18. P.V. Braun, P. Osenar, M. Twardowski, G.N. Tew, S.I. Stupp, Macroscopic nanotemplating of semiconductor films with hydrogen-bonded lyotropic liquid crystals. *Adv. Funct. Mater.* **15**, 1745 (2005)
 19. A. Trajkovska-Petkoska, R. Varshneya, T.Z. Kosc, K.L. Marshall, S.D. Jacobs, Enhanced electro-optic behavior for shaped polymer cholesteric liquid-crystal flakes made using soft lithography. *Adv. Funct. Mater.* **15**, 217 (2005)
 20. H. Dislich, Sol-gel: science, processes and products. *J. Non-Cryst. Solids* **80**, 115 (1986)
 21. S.P. Mukherjee, Sol-gel processes in glass science and technology. *J. Non-Cryst. Solids* **42**, 477 (1980)
 22. S.S. Sharma, K. Nomura, Y. Ujihira, Mössbauer studies on tin-bismuth oxide CO selective gas sensor. *J. Appl. Phys.* **71**, 2000 (1992)
 23. H. Liu, A. Vajpayee, C.D. Vecitis, Bismuth-doped tin oxide-coated carbon nanotube network: improved anode stability and efficiency for flow-through organic electrooxidation. *ACS Appl. Mater. Interfaces* **5**, 10054 (2013)
 24. J. Yang, S. Pi, Y. Han, R. Fu, T. Meng, Q. Zhang, Characteristic of bismuth-doped tin oxide thin-film transistors. *IEEE Trans. Electron Devices* **63**, 1904 (2016)
 25. L. Leontie, M. Caraman, M. Alexe, C. Harnagea, Structural and optical characteristics of bismuth oxide thin films. *Surf. Sci.* **507–510**, 480 (2002)
 26. S. Condurache-Botam, N. Tigau, A.P. Rambu, G.G. Rusu, G.I. Rusu, Optical and electrical properties of thermally oxidized bismuth thin films. *Appl. Surf. Sci.* **257**, 10545 (2011)
 27. L. Yang, A. Münchinger, M. Kadic, V. Hahn, F. Mayer, E. Blasco, C. Barner-Kowollik, M. Wegener, On the Schwarzschild effect in 3D two-photon laser lithography. *Adv. Opt. Mater.* **7**, 1901040 (2019)
 28. D. Radtke, U.D. Zeitner, Laser-lithography on non-planar surfaces. *Opt. Express* **15**, 1167 (2007)
 29. K.Y. Han, T. Miyashita, T. Uchida, Accurate measurement of the pretilt angle in a liquid crystal cell by an improved crystal rotation method. *Mol. Cryst. Liq. Cryst. Sci. Technol. A* **241**, 147 (1994)
 30. V.S. Dharmadhikari, S.R. Sainkar, S. Badrinarayan, A. Goswami, Characterisation of thin films of bismuth oxide by X-ray photoelectron spectroscopy. *J. Electron Spectrosc. Relat. Phenom.* **25**, 181 (1982)
 31. W. Xiaohong, Q. Wei, H. Weidong, Thin bismuth oxide films prepared through the sol-gel method as photocatalyst. *J. Mol. Catal. A-Chem.* **261**, 167 (2007)
 32. A. W. Adamson, Physical Chemistry of Surfaces. *Physical Chemistry of Surfaces, 5th ed.* (Wiley-Interscience, New York, 1990)
 33. J. Li, Y. Pan, C. Xiang, Q. Ge, J. Guo, Low temperature synthesis of ultrafine α - Al_2O_3 powder by a simple aqueous sol-gel process. *Ceram. Int.* **32**, 587 (2006)
 34. H.-C. Jeong, J.H. Lee, J. Won, B.Y. Oh, D.H. Kim, D.W. Lee, I.H. Song, Y. Liu, D.-S. Seo, One-dimensional surface wrinkling for twisted nematic liquid crystal display based on ultraviolet nanoimprint lithography. *Opt. Express* **27**, 18096 (2019)
 35. H.C. Ling, M.F. Yan, W.W. Rhodes, High dielectric constant and small temperature coefficient bismuth-based dielectric compositions. *J. Mater. Res.* **5**, 1752 (1990)
 36. A.R. Babar, S.S. Shinde, A.V. Moholkar, K.Y. Rajpure, Electrical and dielectric properties of co-precipitated nanocrystalline tin oxide. *J. Alloys Compd.* **505**, 743 (2010)
 37. M. Diantoro, A.A. Kholid, Yudiyanto Mustikasari, The influence of SnO₂ nanoparticles on electrical conductivity, and transmittance of PANI-SnO₂ films. *IOP Conf. Ser. Mater. Sci. Eng.* **367**, 012034 (2018)
 38. S. Chisca, I. Sava, V. Musteata, M. Bruma, Dielectric and conduction properties of polyimide films. *CAS 2011 Proceedings (2011 International Semiconductor Conference)* 253 (2011)
 39. N.J. V, S.P. Rajeev, S. Varghese, Ferroelectric polymer nanocomposite alignment layer in twisted nematic liquid crystal devices for reducing switching voltage. *Liquid Cryst.* **46**, 736 (2019)
 40. Y.-F. Wang, Y.-Q. Guo, Y.-X. Ren, M.-Z. Fu, J.-L. Zhu, Y.-B. Sun, Study on polyvinylidene fluoride as alignment layer in twist-nematic liquid crystal display. *Liquid Cryst.* **45**, 857 (2018)

Publisher's Note Springer Nature remains neutral with regard to jurisdictional claims in published maps and institutional affiliations.